

# Digital confocal microscope

Alexandre S. Goy\* and Demetri Psaltis

Optics Laboratory, École Polytechnique Fédérale de Lausanne, Station 17, Lausanne, 1015, Switzerland  
\*alexandre.goy@epfl.ch

**Abstract:** We demonstrate experimentally a scanning confocal microscopy technique based on digital holography. The method relies on digital holographic recording of the scanned spot. The data collected in this way contains all the necessary information to digitally produce three-dimensional images. Several methods to treat the data are presented. Examples of reflection and transmission images of epithelial cells and mouse brain tissue are shown.

©2012 Optical Society of America

OCIS codes: (180.1790) Confocal microscopy; (090.1995) Digital holography.

---

## References and links

1. M. Minsky, "Microscopy apparatus," US Patent 3,013,467 (1961).
2. C. Sheppard and D. Shotton, *Confocal Laser Scanning Microscopy* (Oxford, BIOS Scientific Publishers 1997).
3. Y. C. Liu and A. S. Chiang, "High-resolution confocal imaging and three-dimensional rendering," *Methods* **30**(1), 86–93 (2003).
4. S. J. Tseng, Y. H. Lee, Z. H. Chen, H. H. Lin, C. Y. Lin, and S. C. Tang, "Integration of optical clearing and optical sectioning microscopy for three-dimensional imaging of natural biomaterial scaffolds in thin sections," *J. Biomed. Opt.* **14**(4), 044004 (2009).
5. M. J. Booth, "Adaptive optics in microscopy," *Philos. Transact. A Math. Phys. Eng. Sci.* **365**(1861), 2829–2843 (2007).
6. J. M. Girkin, S. Poland, and A. J. Wright, "Adaptive optics for deeper imaging of biological samples," *Curr. Opin. Biotechnol.* **20**(1), 106–110 (2009).
7. F. Charrière, A. Marian, F. Montfort, J. Kuehn, T. Colomb, E. Cuche, P. Marquet, and C. Depeursinge, "Cell refractive index tomography by digital holographic microscopy," *Opt. Lett.* **31**(2), 178–180 (2006).
8. K. Dillon and Y. Fainman, "Computational confocal tomography for simultaneous reconstruction of objects, occlusions, and aberrations," *Appl. Opt.* **49**(13), 2529–2538 (2010).
9. N. Lue, W. Choi, K. Badizadegan, R. R. Dasari, M. S. Feld, and G. Popescu, "Confocal diffraction phase microscopy of live cells," *Opt. Lett.* **33**(18), 2074–2076 (2008).
10. G. Barbastathis, M. Balberg, and D. J. Brady, "Confocal microscopy with a volume holographic filter," *Opt. Lett.* **24**(12), 811–813 (1999).
11. C. Yang and J. Mertz, "Transmission confocal laser scanning microscopy with a virtual pinhole based on nonlinear detection," *Opt. Lett.* **28**(4), 224–226 (2003).
12. E. Cuche, P. Marquet, and C. Depeursinge, "Spatial filtering for zero-order and twin-image elimination in digital off-axis holography," *Appl. Opt.* **39**(23), 4070–4075 (2000).
13. S. G. Johnson and M. Frigo, "A modified split-radix FFT with fewer arithmetic operations," *IEEE Trans. Signal Process.* **55**(1), 111–119 (2007).
14. D. J. Brady, K. Choi, D. L. Marks, R. Horisaki, and S. Lim, "Compressive holography," *Opt. Express* **17**(15), 13040–13049 (2009).

---

## 1. Introduction

Confocal microscopy is a well established optical imaging method because of its three-dimensional sectioning capability [1, 2]. The original proposal by Minsky relied on linear scattering and absorption of the sample as the contrast mechanism, however, confocal microscopy has found more widespread use in fluorescence imaging. The advantage of fluorescence confocal imaging is that fluorophores can label specific biological targets and also that it provides a strong contrast mechanisms that does not rely on scattering. On the other hand, when we measure the linear scattering and absorption properties of a 3D sample in the confocal geometry, the same inhomogeneities we attempt to measure distort the probing beam leading to image degradation. Several techniques have been proposed to improve the image quality by reducing the scattering of the tissue by matching the refractive index with specific clearing agents [3, 4] or through adaptive optics, which can improve the quality of the probing beam and correct for sample-induced distortion [5, 6]. Other methods

such as phase tomography [7, 8] and quantitative phase imaging [9] have been developed to produce three-dimensional images using only the scattering properties of the sample.

The method we demonstrate in this letter allows the dynamic placement of a virtual pinhole in order to suppress part of the sample-induced aberrations. It also enables a convenient implementation of transmission confocal microscopy, as no de-scan mechanism is required to steer the scanned beam through the detection pinhole. In order to suppress the pinhole on the detection side, it has been previously proposed to replace it by a volume hologram [10] or use an intense laser together with a nonlinear crystal to track the focus position by detection of the second harmonic generated light [11].

Our method allows us to dynamically locate the focus in three dimensions by the capture of a digital hologram. The data is processed in real time by simulating the light propagation in a conventional confocal microscope. The fact that the data is available in the digital domain makes it possible to optimize the location and size of the virtual pinhole and select other metrics to obtain contrast, other than the amount of light transmission through a fixed pinhole. We demonstrate these methods on experimental data and produce both reflection and transmission confocal images.

## 2. Method

The experimental apparatus we use for our experiments is shown in Fig. 1(a). The general structure is that of a double interferometer for reflection and/or transmission imaging. The set-up is symmetric. The sample and imaging optics are placed in the signal arm. The back focal plane of the objective is imaged with unit magnification onto a camera by two relay lenses of 100mm focal length, L1 and L2 (L3 and L4 in reflection). Lens MO2, a 100x oil immersion objectives with a numerical aperture of 1.4 (Olympus UPlansApo), focuses the illumination on the sample and the position of the focused spot in scanned in three dimensions by translating the sample. The light transmitted through the sample is collected by lens MO1, which is the same as MO2. The laser source is a continuous wave laser diode at 405nm. The illumination power onto the sample is 10 $\mu$ W. The coherence length of the diode is 100 $\mu$ m which is used to remove the parasitic reflections from the objective. We record separate digital holograms on the cameras for each scanning position using off-axis digital holography [12]. The camera on the transmission side (CCDt on Fig. 1) is a Scion CFW-1312M CCD with 4.65 $\mu$ m pixels and a resolution of 1360 by 1024 pixels binned two by two in order to provide effective pixels of 9.3 $\mu$ m. The camera on the reflection side (CCDr on Fig. 1) is an Andor iXon885 CCD with 1002 by 1004 8 $\mu$ m pixels. Both cameras are triggered by the computer in order to retrieve simultaneous snapshots of the transmitted and reflected beams. The image acquisition is synchronized to the translation stage, which moves continuously. The snapshot frequency is set at 4Hz and the integration is set to 10ms to limit the motion blur while the sample is scanned. The scanning speed depends on the desired resolution and ranges between 1 and 4 $\mu$ m/s for the experiments presented here. For comparison purposes, the virtual confocal can be turned into a conventional confocal microscope by putting a pinhole with a photodetector at the focus between lenses L1 and L2, as depicted on Fig. 1(b).

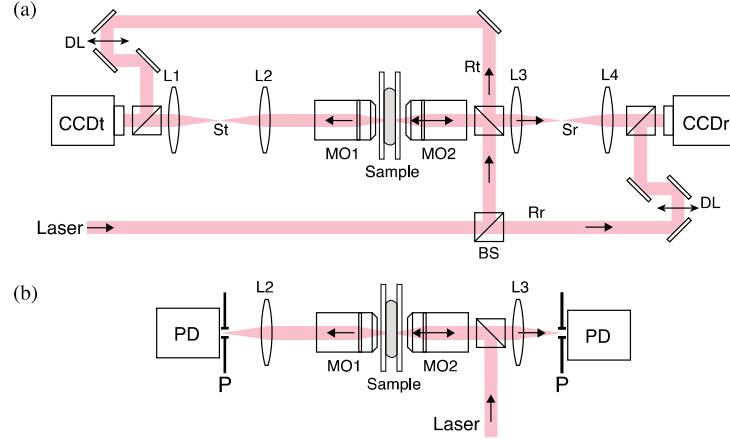


Fig. 1. (a) Optical set-up for digital holographic confocal microscopy. A reference beam  $R_t$  (resp.  $R_r$ ) is extracted for the transmission (resp. reflection) hologram. The sample, sealed between two cover slips, is placed between two microscope objectives (MO1 and 2) and scanned using a 3D translation stage. The back focal plane of objective MO1 (resp. MO2) is imaged on camera CCDt (resp. CCDr) using two relay lenses L1 and L2 (resp. L3 and L4) in a 4f configuration. The optical Fourier transform of the focus is produced on the camera in transmission (resp. reflection). The reference beam is introduced off-axis using a second beam splitter. (b) Modified set-up for conventional confocal imaging with a pinhole of  $50\mu\text{m}$  in front of the detector.

The following procedure is applied separately to reflection and transmission holograms. Using the usual convention, the direction denoted by  $x$  and  $y$  are perpendicular to the direction of propagation. The propagation direction is denoted by  $z$ . The complex field extracted from the hologram is a two dimensional array and is Fourier-transformed using the fast Fourier transform (FFT) algorithm. To improve the efficiency of the FFT, square areas of 512 by 512 pixels containing most of the signal are extracted from the images provided by the cameras. Denoting the reference and signal field by  $r$  and  $s$  respectively, the intensity of the hologram captured on the CCD is given by  $I_h = |r + s|^2$ . The reference intensity  $|r|^2$  and incidence angle are known and the reference can be expressed as  $r = |r|\exp[i(\kappa_x x + \kappa_y y)] \exp[ik(x^2 + y^2)/(2R)]$ , where  $\kappa_x$  and  $\kappa_y$  are the horizontal and vertical spatial frequencies of the fringes. The last term accounts for any remnant curvature of the reference wavefront of radius  $R$ . The signal wave  $s$  is collinear to the optical axis. We calculate  $\text{FFT}\{r I_h\} = \text{FFT}\{r|r|^2 + r|s|^2 + r^2 s^* + |r|^2 s\}$  and we digitally filter out the DC term ( $r|r|^2 + r|s|^2$ ) and the conjugate image  $r^2 s^*$ . We then filter the signal  $|r|^2 s$  with a circular aperture, which acts as a virtual pinhole. If the reference is flat and wide enough, it can be considered constant and  $\text{FFT}\{|r|^2 s\} \approx |r|^2 \text{FFT}\{s\}$ , where the approximation is due to any spatial variations in  $r$ . The confocal signal  $I_{conf}$  is the intensity integrated within the pinhole:

$$I_{conf} = \sum_{k_x, k_y \in \text{pinhole}} \left| \text{FFT}\{s\}_{k_x, k_y} \right|^2 \quad (1)$$

The diameter of the virtual pinhole is calculated as follows. The relay lenses L1 and L2 in a 4f configuration replicate the field in the back focal plane of the imaging objective onto the camera. The camera plane is the Fourier transform of the plane inside the sample where the light comes to focus. By taking a Fourier transform of the data from the camera, we get back to the spatial domain, where the light has to focus through the confocal pinhole (see Fig. 2(a)). In the virtual pinhole plane, the diameter of the pinhole is given by (in pixel units):

$$\tilde{D}_{opt} = \frac{N \Delta x}{\lambda f} D_{opt} = 1.22 \frac{N \Delta x}{N A f} \quad (2)$$

where  $D_{opt} = 1.22 \lambda / N.A.$  is the optimal diameter of the pinhole in physical units,  $N$  is the width and height of the image,  $\Delta x$  is the size of the camera pixels,  $N.A. = 1.4$  is the numerical aperture of the imaging objective and  $f = 1.8\text{mm}$  is its focal length. For the camera in reflection, we have  $N = 512$  and  $\Delta x = 8\mu\text{m}$ , which gives  $\tilde{D}_{opt} = 2.0$ . In transmission the  $4.65\mu\text{m}$  pixels are binned in order to make  $9.3\mu\text{m}$  pixels, we have then  $N = 512$  and  $\Delta x = 9.3\mu\text{m}$ , which gives  $\tilde{D}_{opt} = 2.3$ . For both images, in reflection and in transmission, we selected a 2 by 2 pixel window centered around the maximum of the focus spot. Note that, by zero-padding the hologram to a larger image ( $N$  larger), it is possible to increase the resolution in the Fourier space and smoothen the image, but this requires a longer time to process.

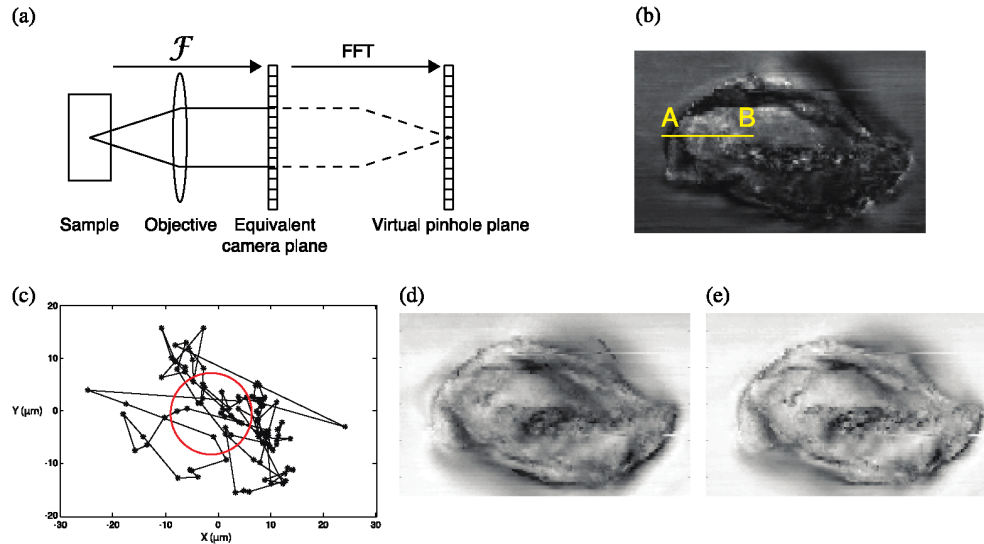


Fig. 2. Digital hologram filtering with the virtual pinhole. (a) Schematic of the virtual confocal principle: the field on the camera is the Fourier transform of the focus in the sample. The field is discretized by the CCD array as suggested by the drawing. This data is Fourier transformed in the computer to simulate the lens that would focus the light through the pinhole. (b) Transmission digital confocal image of an epithelial cell obtained by using a fixed pinhole. (c) Graph showing the motion of the image of the focus in the XY plane due to aberration as the sample is scanned along line A-B on picture (b). The circle represents the pinhole. (d) Corrected image obtained by tracking the focus in three dimension. (e) Corrected image obtained by performing the correlation between the measured focus and an ideal Gaussian beam.

In a conventional confocal microscope in transmission, the alignment of the pinhole is difficult. A few alignment and imaging iterations are required to maximize the contrast of the image. In the case of the digital (holographic) confocal microscope, the alignment of the virtual pinhole is best done in the digital domain. In order to focus digitally the interference term of the hologram  $r*s$ , we need to multiply it by  $r$  and then take the FFT. However, there is, in the experiment, some uncertainty about the exact phase of  $r$  (both in angle and sphericity). Moreover, the signal term itself can have some remnant phase curvature due to aberrations and/or misalignment. Therefore, the first step in the procedure is to iteratively modify  $r$  to compensate for angle and sphericity until a focussed spot is obtained at the expected position in the digital reconstruction. We used a custom digital holography software that displays the extracted phase in real-time to visually adjust the off-axis reference angle, which amounts to bring the Fourier transform of the beam to the center of the Fourier plane where the virtual pinhole lies. This alignment procedure is performed while the beam passes next to the sample in a zone free from scattering. The aberrations that may be due to the cover

slips when we scan the sample are thus also present during alignment. However, it is true that the focus may move slightly when we scan over several tens of microns. This issue is solved by pre-recording the reference angles needed to keep the focus in the center of the Fourier plane as a function of the scan position. Once this operation is complete, the optimal angle of incidence and the curvature of the reference are recorded and applied for the virtual confocal measurement.

The key advantage of the digital confocal method is that the pinhole can be placed dynamically as the object is scanned. The useful signal is the light scattered from the focus within the sample. In transmission, any deflection of the probe beam induces distortions when gated by a fixed pinhole. Lensing effects in the sample may also move the focus in the  $Z$  direction. To perform the dynamic placement of the pinhole, we first calculate the field in the ideal plane of the pinhole, i.e. where the light would focus if it was not deviated by the sample. In this plane, the focus may not be sharp because of lensing effects. We perform a Fourier beam propagation along the  $Z$  direction to determine the three-dimensional distribution of the optical field in the vicinity of the ideal pinhole plane. In each  $XY$  plane along the propagation, we perform a correlation operation (hereafter called Gaussian correlation) between the measured focus and an ideal Gaussian focus that would have been obtained through a clear medium. For each plane, the monitored value is the maximum of the correlation function, which gives an estimate of the amount of light scattered at the focus within the sample. From this, we select the  $XY$  plane  $P_{opt}$  where the correlation reaches its maximum along the  $Z$  direction and we center the virtual pinhole on the centroid of the focus spot. The plotted value is the integrated intensity that passes through the pinhole. An improved image of the sample can also be produced by plotting the maximum value of the Gaussian correlation in plane  $P_{opt}$  for each scanned point.

When the pinhole follows the image of the focus in three dimensions, it selects the useful scattered light that has traveled together with the probe beam. The probe beam becomes a constant background and does not contribute to the signal any more. As a result, the images are cleaned from most of the shading effect, as exemplified on Fig. 2.

### 3. Sample preparation

We demonstrated the technique on two different samples that were mounted between two 150 $\mu\text{m}$ -thick glass cover slips and sealed with nail polish. The samples were attached on a three-dimension translation stage (Newport UTS50CC). The first sample was a buffered 10% formaldehyde solution with dispersed human epithelial mouth cheek cells. These cells are ovoid and 50 to 60 $\mu\text{m}$  in size. The space between the two cover slips was 25 $\mu\text{m}$  and, as a result, the cells were immobilized. This sample has negligible absorption and was thin enough to be placed between the two objectives MO1 and MO2 shown in Fig. 1(a). In this case, we could image in reflection and transmission simultaneously.

The second sample was a 200 $\mu\text{m}$  thick slice of mouse brain tissue in a buffered 10% formaldehyde solution. The brain tissue was too thick to be imaged in transmission but reflection imaging was demonstrated down to a depth of 40 $\mu\text{m}$ . The maximal depth that one can reach, in principle, depends on the scattering properties of the tissue.

### 4. Results

Three reflection scans of the mouse brain tissue are presented in Fig. 3, each with and without the virtual pinhole. The first two are  $XY$  sections and the third one is a  $XZ$  section ranging over 40 $\mu\text{m}$  in  $Z$ . The dark spots are the nuclei of the cells and large fibrous structures are visible. The pinhole has a dramatic effect on the resolution by rejecting out of focus light. This demonstrates the efficiency of the principle of confocal imaging in this case.

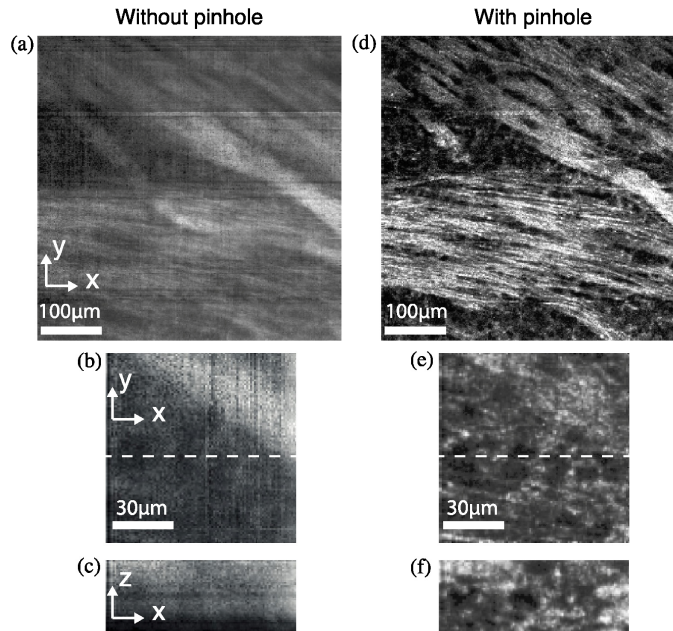


Fig. 3. Mouse brain tissue images. (a) 500µm by 500µm XY section 20µm deep in the tissue, without pinhole filtering. (b) 100µm by 100µm XY section close to the center of image (a), without the pinhole. (c) XZ section, Z coordinate ranging from 0 to 40µm in depth. The trace of the section in the XY plane is shown by the dashed line on image (b). (d) (e) and (f) Images corresponding to (a), (b) and (c) respectively, obtained with pinhole filtering. The scanning step for all sections is 1µm.

In Fig. 4, we show three sections of the epithelial cells obtained with the digital confocal microscope in reflection. We see the nucleus appearing as we scan. The slices are spaced by 5µm from each other in Z. In Fig. 5, we show results from the same cell as in Fig. 4 for the transmission geometry. Images in Fig. 5(a) to 5(c) are the same section as in Fig. 4 without any compensation for movements of the focus. Figure 5(d) to 5(f) show images obtained with dynamic pinhole placement. Figure 5(g) to 5(i) show images obtained using the Gaussian correlation metric.



Fig. 4. (a) to (c) Three successive XY sections in a human epithelial cell. The sections are spaced by 5µm in Z. The images have been obtained in reflection using the digital confocal microscope.

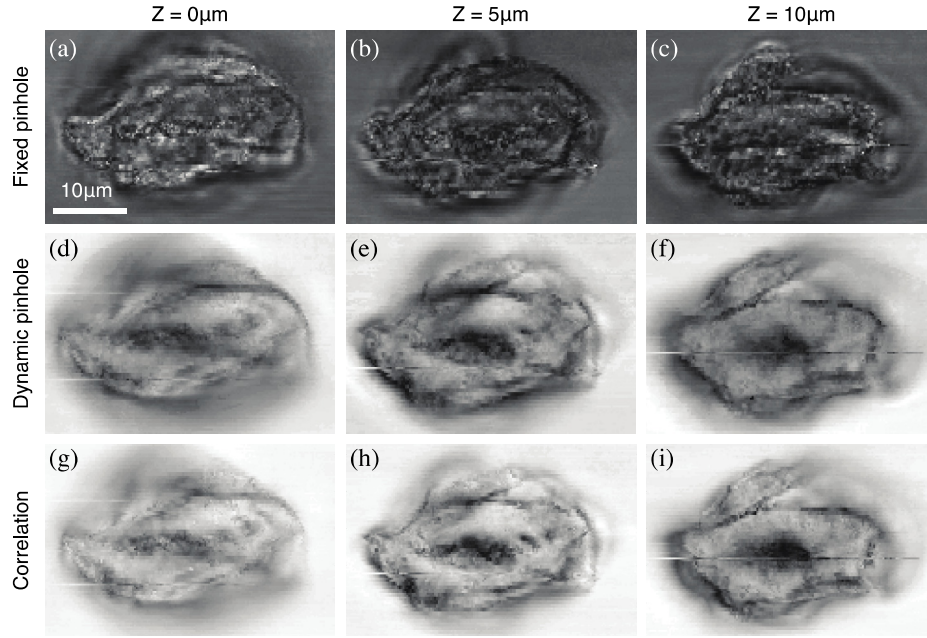


Fig. 5. (a) to (c) Images of the same cell as in Fig. 4, obtained with digital confocal in transmission without dynamic pinhole placement. The sections are spaced by  $5\mu\text{m}$  in  $Z$ . (d) to (f) Transmission images obtained with dynamic placement of the virtual pinhole. (g) to (i) Transmission images obtained using the Gaussian correlation metric.

Figure 6 shows the cell displayed in Fig. 4 and 5 in the XZ plane. The positive effect of the dynamic pinhole placement is clearly evident in the transmission geometry when we compare Fig. 6(b) and 6(c). The dynamic pinhole placement and Gaussian correlation methods produced comparable results in this case.

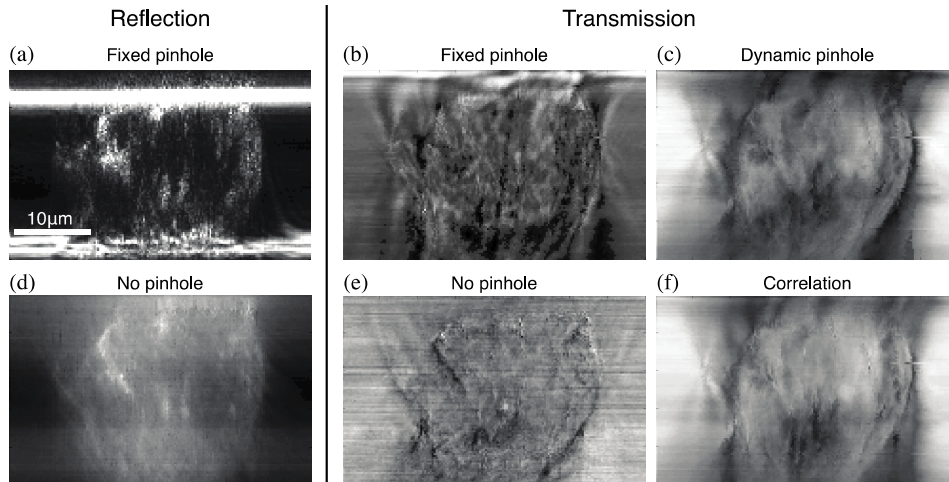


Fig. 6. (a) Reflection digital confocal XZ section with fixed pinhole of the cell shown in Fig. 4 and 5. The two horizontal lines correspond to the interfaces between the coverslips and the water solution. (b) Transmission digital confocal image with fixed virtual pinhole. (c) Transmission confocal section obtained by tracking the focus in three dimensions with the virtual pinhole. (d) and (e) Reflection and transmission sections respectively without virtual pinhole. (f) Transmission section obtained using the Gaussian correlation.

## 5. Discussion

The dynamic placement of the pinhole provides a significant improvement of the images obtained in transmission because the scattered wave is weak in comparison to the probe beam. As the pinhole tracks the image of the focus spot, the strong contribution of the latter reduces to a constant background. The pinhole filters the scattered light around the image spot and reveals information about the light scattered at the focus within the sample. In reflection, the light gets reflected on refractive index gradients. As most of the reflected power comes from the focus, the light rays will trace back on themselves making reflection imaging less sensitive to distortion.

The speed of digital confocal images acquisition is limited by the frame rate of the camera and by the time required for processing the data. Calculating the full FFT for each frame is not necessary as only the values within the aperture of the virtual pinhole contribute to the signal. We can evaluate the number of real floating point operations (addition and multiplication needed) for each frame. For each one of the  $N_p$  pixels within the pinhole, we need to perform the following summations over the pixels in the image:

$$p = \sum_{x,y} F_{xy} \cos(k_x x + k_y y) + i \sum_{x,y} F_{xy} \sin(k_x x + k_y y) \quad (3)$$

where  $F_{xy}$  is the image. The arrays  $\cos(k_x x + k_y y)$  and  $\sin(k_x x + k_y y)$  can be calculated in advance and stored in the memory. After the summation, we add the intensities of the pixels in the pinhole, which requires  $4N_p - 1$  operations ( $N_p$  squaring operations for both the real and imaginary parts and  $2N_p - 1$  additions of all the squares). For a square image of size  $N$  by  $N$ , the total number of operation is  $N_{op} = 3N_p N^2 + 4N_p - 1$ . Note that for  $N_p < 25$ , this is smaller than the number of operations for a FFT which in the order of  $2N(34/9 N \log_2 N)$  [13]. In our experiment,  $N_p = 4$ ,  $N = 480$  and  $N_{op} = 2,764,815$ . Computation speed on graphic processing units is now in the range of  $10^{12}$  floating point operations per second. Since the operations required can be made completely parallel, this allows us to process 36,000 frames per second. Among the fastest commercially available devices, some high-end cameras achieve 25,000fps for 512x512 pixel images. This corresponds to 12 scanned slices per second for a standard VGA resolution of 640x480 pixels. To achieve such a speed we would have to scan the laser focus rather than the sample. This adds complication since we have to account for the change in angle of the signal beam. Fortunately, in the digital approach, the angles can be digitally recorded during an initial calibration phase and used in subsequent imaging.

## 6. Conclusion

We have experimentally demonstrated a scanning confocal microscopy technique, in reflection and transmission, based on the numerical treatment of digital holograms in real time for each scanned spot. The results reported here might open up interesting avenues for future research. The data collected with the scanning digital holographic set-up is a complete record of the information that can be gathered within a given numerical aperture, from the scattering by the object of the coherent field. The fact that this information is available in the digital domain gives us the flexibility to process and interpret the data in a variety of ways. For example, we presented the Gaussian correlation method as an alternative to the dynamic virtual pinhole approach. For sparse objects, we expect that compressive sampling technique [14] will work particularly effectively. This will be the subject for a future paper.